Stochastic Characteristics of Temperature-Dependent MEMS-Based Inertial Sensor Error

M. El-Diasty, York University
A. El-Rabbany, Ryerson University
S. Pagiatakis, York University

BIOGRAPHY

Mohammed El-Diasty is a PhD candidate in the Department of Earth & Space Science & Engineering at York University, Canada. He received a MASc degree in Civil Engineering from Ryerson University, Canada and a BSc in Civil Engineering from Mansoura University, Egypt. His current research focuses on the development of an integrated MEMS-Based INS/GPS system for marine applications.

Dr. Ahmed El-Rabbany is an associate professor of Geomatics Engineering at Ryerson University. He holds a Ph.D. degree in GPS from the Department of Geodesy and Geomatics Engineering, University of New Brunswick. Dr. El-Rabbany serves as the Geodesy councilor of the Canadian Institute of Geomatics and chair of its Toronto Branch.

Dr. Spiros Pagiatakis is associate professor of Geodesy and Geomatics Engineering in the Department of Earth and Space Science and Engineering at York University in Toronto. He has a BSc in Surveying Engineering from the National Technical University of Athens (Greece) and an MSc and PhD from the University of New Brunswick. Dr. Pagiatakis is interested in the dynamics of the Earth as observed by geodetic techniques, physical geodesy, ocean tide loading and in spectral methods for the analyses of geophysical time series.

ABSTRACT

The GPS/INS integrated system has been widely used in hydrographic surveying for positioning and orientation purposes. However, existing systems use high-end inertial sensors, which are very expensive and bulky. To overcome the cost and size of inertial sensors, Micro-Electro-Mechanical System (MEMS)-based inertial technology is proposed. A major drawback of low-coast MEMS-based inertial sensors however, is that their output signals are contaminated by high-level noise. In addition, because of their miniature size, MEMS sensors are very sensitive to ambient environmental conditions, (e.g. temperature), which cause the sensor to exhibit large, rapidly changing errors. Unless the high frequency noise component is suppressed, and accurate temperature-dependent stochastic model is built, optimization the filtering methodology cannot be achieved.

This paper examines the effect of varying the temperature points on the MEMS inertial sensors' noise models using Allan variance and Least-Squares Spectral Analysis (LSSA). Allan variance is a method of representing root mean square random drift error as a function of averaging times. LSSA is an alternative to the classical Fourier methods and has been applied successfully by a number of researchers in the study of the noise characteristics of experimental series. Static data sets are collected under different temperature points using two MEMS-based IMUs, namely MotionPakII and Crossbow AHRS300CC. The performance of different MEMS inertial sensors is predicted from the Allan variance estimation results at different temperature points and the LSSA is used to study the noise characteristics and define the sensors' stochastic model parameters. It is shown that the stochastic characteristics of MEMS-based inertial sensors can be identified using Allan variance estimation and LSSA and the sensors' stochastic model parameters are temperature-dependent. Also, the Kaiser Window FIR low pass filter is used to investigate the effect of de-noising stage on the stochastic model. It is shown that the stochastic model is also dependent on the chosen cut-off frequency.

1. INTRODUCTION

The performance of a GPS/INS integrated system is mainly characterized by the ability of INS to bridge GPS outages. This basically depends on the inertial sensor errors, which, if not treated, cause a rapid degradation in the INS navigation solution during the periods of GPS outages. The inertial sensor errors can be divided into two parts, deterministic (systematic) errors and random errors (Nassar, 2002). In order to integrate MEMS inertial sensors with GPS, and to provide a continuous and reliable navigation solution, the characteristics of different error sources and the understanding of the stochastic variation of these errors are of significant importance (Park, 2004).

The deterministic error sources include the bias and the scale factor errors which can be removed by specific calibration procedures in a laboratory environment. Park (2004) discusses the laboratory calibration procedure for MEMS inertial sensors, whereas Shin (2001) developed field calibration procedures. Abdel-Hamid et al., (2003) and Abdel-Hamid (2005) implemented the deterministic error (bias and scale factor) to MEMS IMU at different temperature points and demonstrated that deterministic error is temperature-dependent.

The inertial sensor random errors primarily include the sensor noise, which consists of two parts, a high frequency component and a low frequency component. The high frequency component has white noise characteristics, while the low frequency component is characterized by correlated noise (Skaloud, 1999). De-noising methodology is required to filter the high frequency noise in the inertial sensor measurements prior to processing, using a low pass filter or a wavelet de-noising technique. Several studies have focused on evaluating the advantages of such techniques (e.g., Skaloud (1999), Nassar (2002), and Abdel-Hamid et al. (2004)). In this paper the Kaiser Window FIR low pass filter is used with the same specifications in Skaloud (1999). Skaloud (1999) used 8 Hz cut-off frequency, 0.0001 dB pass-band attenuation, 100 dB stop-band attenuation and claimed that broader transition band is not as critical as achieving good attenuation in the stop-band. Furthermore, attenuation in stop-band is not so critical since this part of the spectrum contains a relatively small part of the total signal power (Skaloud, 1999).

The low frequency noise component (correlated noise) can be modeled with sufficient accuracy using random processes (Nassar, 2002), such as, random constant (random bias), random walk, Gauss-Markov or periodic random processes. Details of these stochastic models can be found in Gelb (1974) and Nassar (2002). The most commonly used process is the first order Gauss Markov process whereas more recently, the use of Auto-Regressive (AR) modeling methods for low cost sensors was tested (e.g., Nassar, 2002; Park, 2004). Moreover, Hou (2004) used Allan variance to study the random error and demonstrated that the most dominant error is random walk for MEMS-based IMU. However, one specific limitation of most of these investigations is that the stochastic variation of these errors, which is of significant importance, has not been investigated at different temperature points. The process of understanding the stochastic variation at different temperature points is one of the most important steps for developing a reliable low cost integrated navigation system. The reason is that the low cost IMU propagates relatively large navigation errors in a small time interval. Unless an accurate temperature-dependent stochastic model is developed, the mechanization parameters will have higher error and could potentially degrade system performance.

In this work we collect static data sets under different temperature points using two MEMS-based IMUs, namely MotionPakII and Crossbow AHRS300CC. The performance of different MEMS inertial sensors is predicted from the Allan variance estimation results at different temperature points and the LSSA is used to study the noise characteristics and define the sensors' stochastic model parameters. It is shown that the stochastic characteristics of MEMS-based inertial sensors can be identified using Allan variance estimation and LSSA and the sensors' stochastic model parameters are temperature dependent.

2. METHEDOLOGIES

To evaluate the temperature effect on the stochastic model, the data are analyzed using the Allan variance and Least squares spectrum. Also, the effect of de-noising at different cut-off frequencies on the stochastic model is implemented. The algorithms used are:

- Allan Variance;
- Least square Spectrum ,
- Kaiser Window FIR Low Pass Filter Design.

Below is the brief description of these techniques.

2.1. Allan Variance

The Allan variance is a method of representing root mean square random drift error as a function of averaging times. It is simple to compute, much better than having a single RMS drift number to apply to a system error analysis, relatively simple to interpret and understand. Its most useful application is in the identification and estimation of random drift coefficient in a previously formulated model equation. If N is the number of data points with sampling internal of t_0, then a group of n data points (with n<N/2) can be created. Each group member is called a cluster T and is equal to nt_0. The Allan variance can be defined in terms of output variable, calculated at discrete times $x_k=x(kt_0)$. The Allan variance is estimated as follows (IEEE Std. 647-1995, 1998; Hou and El-Sheimy, 2003):

$$\sigma^2(T)=\frac{1}{2T^2(N-2n)}\sum_{k=1}^{N-2n}(x_{k+2n}-2x_{k+n}+x_k)^2 \qquad (1)$$

There is a very important relationship between Allan variance and power spectral density (PSD) of the random processes:

$$\sigma^2(T)=4\int_0^\infty df\cdot S_R(f)\cdot\frac{\sin^4(\pi fT)}{(\pi fT)^2} \qquad (2)$$

where $S_R(f)$ is the power spectral density of the random process $R(T)$, namely the instantaneous output rate of the

sensor. In the derivation of Equation (2), it is assumed that the random process $R(T)$ is stationary. Equation (2) is the key result that will be used to calculate the Allan variance from the rate noise PSD. The different types of random processes can be examined by investigating Allan variance plot. The Allan variance provides a means of identifying various noise terms that exist in the data. Typical Allan variances plot looks like the one shown in Figure 1 (IEEE Std. 647-1995, 1998; Hou and El-Sheimy, 2003).

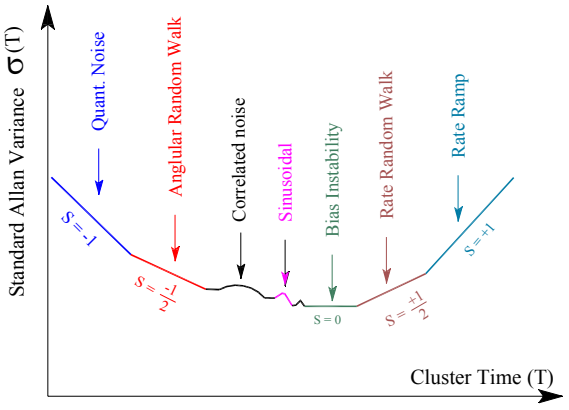

Figure 1 $\sigma(T)$ Allan variance analysis noise terms results (after IEEE Std. 952-1995, 1998)

It should be noted that the different noise terms appear in different regions of T. This property permits easy identification of various random processes that exist in the data. For instance, the random walk process can be identified at T equal to 1h and with a straight line of slope -1/2 as shown in Figure 1. The noise PSD rate is represented by (IEEE Std. 647-1995, 1998):

$$S_{\Omega}(f)=Q^2 \tag{3}$$

where Q is the angular random walk coefficient. Substituting Equation (3) in Equation (2) and performing the integration results:

$$\sigma^2(T)=\frac{Q^2}{T} \tag{4}$$

Equation (4) indicates that a log-log plot of $\sigma(T)$ versus T has a slope of –1/2. Also, Q can be estimated by reading the slope line at $T = 1h$. Fore more details refer to IEEE Std. 647-1995 (1998).

2.2. Least Squares Spectral Analysis

Least Squares Spectral Analysis (LSSA) was first developed by Vanícek in 1969. LSSA is an alternative to the classical Fourier methods to overcome all inherent limitations of Fourier techniques. The LSSA provides the following advantages; (1) unwanted periodic signals (i.e., low frequency signals) and systematic noise (i.e., coloured or other) can be suppressed without producing any shift of the existing spectral peaks, (2) statistical testing on the significance of spectral peaks can be performed. It uses the least squares approximation technique, which is closely related to the least squares parametric adjustment (Pagiatakis, 1999). The details of this technique have already been shown by Pagiatakis, (1999).

An observed time series is considered to be represented by $f = f(t) = \{f_i\}, i = 1, 2, \cdots, n$. The main objective is to extract periodic signals in f, especially when f contains both, random and systematic noise. Thus, we can set up a model $\boldsymbol{g}$ that can be expressed as follows:

$$g = \Phi x \tag{5}$$

Where Φ is a matrix of known base functions and x is the vector of unknown parameters. Here we do not assume t_i to be equally spaced. But we assume that the observations $f_i, i = 1, 2, \cdots, n$ possess a fully populated covariance matrix $\mathbf{C_f}$. To estimate the model parameters x, the standard least-squares notation (e.g. Vanícek and Krakiwsky, 1986), in which the difference between $\boldsymbol{g}$ and $\boldsymbol{f}$ becomes minimum. The estimation of the model parameters can be obtained as follows:

$$\hat{x} = (\Phi^{\mathbf{T}} C_f^{-1} \Phi)^{-\mathbf{1}} \Phi^{\mathbf{T}} C_f^{-1} f \tag{6}$$

$$\hat{g} = \Phi\hat{x} = \Phi(\Phi^{\mathbf{T}} C_f^{-1} \Phi)^{-\mathbf{1}} \Phi^{\mathbf{T}} C_f^{-1} f \tag{7}$$

In least-squares method, the model parameters are determined, such that the difference between $\hat{g}$ and $\boldsymbol{f}$ is minimum. Using the standard least-squares (Vanícek and Krakiwsky, 1986) we can write:

$$\hat{v} = f - \hat{g} = f - \Phi(\Phi^{\mathbf{T}} C_f^{-1} \Phi)^{-\mathbf{1}} \Phi^{\mathbf{T}} C_f^{-1} f \tag{8}$$

From the projection theorem we know that $\hat{v} \perp \hat{g}$. This means that $\boldsymbol{f}$ has been decomposed into a signal $\hat{g}$ and noise $\hat{v}$ (residual series). Hence, to describe how $\hat{g}$ represents $\boldsymbol{f}$, we use a fractional measure s that is the ratio of the length of this orthogonal projection to the length of $\boldsymbol{f}$ and can be expressed as follows (Pagiatakis, 1999):

$$s = \frac{f^T C_f^{-1} \hat{g}}{f^T C_f^{-1} f} \tag{9}$$

In spectral analysis we usually try to search for the hidden periodic signals that are expressed in terms of sine and cosine base functions. So, if we specify the form of the base functions to be trigonometric based on a set of spectral frequencies $\omega_i, i = 1, 2, \cdots, m$, we have

$$\hat{g}(\omega_i) = \hat{x}_{1i} \cos \omega_i t + \hat{x}_{2i} \sin \omega_i t. \tag{10}$$

Let $\hat{x} = [\hat{x}_{1i},\ \hat{x}_{2i}]^T$ and $\mathbf{\Phi} = [\cos\omega_i t,\ \sin\omega_i t]$, then $\hat{x}$ can be determined from (5). So for different frequencies ω_i, $i = 1, 2, \cdots, m$, we can get different spectral values. Then the least-squares spectrum is defined by (Pagiatakis, 1999):

$$\mathbf{s}(\omega_i) = \frac{f^{\mathbf{T}} C_f^{-1} \hat{g}(\omega_i)}{f^{\mathbf{T}} C_f^{-1} f} = \left[1 + \frac{Q_n}{Q_s}\right]^{-1} \qquad i = 1, 2, \cdots, m. \quad (11)$$

where Q_n and Q_s are the quadratic forms of the noise and signal respectively. Equation (11) describes the least squares spectrum. Obviously the least squares spectrum of $\boldsymbol{f}$ is the collection of the spectral values for all desired frequencies ω_i, $i = 1, 2, \cdots, m$. The bigger the spectral value at a frequency ω_i, the more powerful $\boldsymbol{f}$ is at this frequency (Pagiatakis, 1999). Also, Equation (11) can be further developed into other forms to provide the researcher with more familiar spectral representations, such as power spectral density (PSD) in decibels (dB) or in units^2/frequency, where "units" signifies the units of the time series values. Following Pagiatakis (1999), the least-squares power spectral density in decibels is given by:

$$PSD_{LS} = 10\log\left[\frac{s}{1-s}\right], \quad (dB) \qquad (12)$$

Solving Equation (11) with respect to Q_s and dividing by the frequency f, the classical least-squares spectrum can be transformed into least-squares PSD in units^2/*f*

$$PSD_{LS} = \frac{Q_n}{f}\left[\frac{s}{1-s}\right], \quad (unit^2 / f) \qquad (13)$$

The least-squares PSD in equations (12) and (13) are equivalent to the determined from the FFT method, when the series is equally spaced and equally weighted. The advantages of equations (12) and (13) are that they can be used to calculate power spectra of any series, without considering the restricted conditions in FFT algorithm.

Generally speaking, the observed time series may include trigonometric base functions in Equation (10) to describe the periodic components of the series, or other, such as random walk and autoregressive (AR) (Gelb, 1974). The above algorithm is implemented in software LSSA v5.20. This software is based on LSSA v1.0 (Wells and Vanícek, 1978) and LSSA v2.0 (Wells et. al., 1985). Statistical evaluation of the results of this analysis is implemented in LSSA v5.2 and based on statistical theorems developed by Pagiatakis (1999) and other classical statistical tests found in geodetic methodology (Mikhail, 1976; Vanícek and Krakiwsky, 1986).

2.3. Kaiser Window FIR Low Pass Filter Design

As mentioned previously, low cost inertial sensors have typically larger error sources than navigation-grade IMUs, which result in huge positioning error if not compensated appropriately. They can be divided into two parts, i.e. random constants (biases, scale factors) and random noise. Calibration can be applied to eliminate random constant errors (Shin, 2001), and low-pass filters are usually applied to remove high frequency random noise. For instance, Skaloud (1999) shows that Butterworth low-pass filters, which are usually used in commercial software, actually affect the azimuth estimation negatively. Skaloud (1999) also used forward/backward Finite Impulse Response (FIR) filters, which don't have phase delay and therefore are most effective for post-processing applications that aim to improve the attitude determination accuracy.

There are two types of filters, i.e., Finite Impulse Response (FIR) and Infinite Impulse Response (IIR) filters. The advantages of FIR filters are their linear phase property and guaranteed stability (Orfanidis, 1996). The procedure to design a low-pass Kaiser FIR filter is different from other windowing techniques in that Kaiser FIR filter has control over the pass-band and stop-band that specifies the deviation error between the frequency response of the output filter and its desired amplitude, δ_{pass} and δ_{stop}, respectively (Orfanidis, 1996).

For the low-pass filters the desired ideal frequency response $G(\omega)$ is defined over the Nyquist interval by:

$$G(\omega) = \begin{cases} 1, & if\ |\omega| \le \omega_c \\ 0, & if\ \omega_c < |\omega| \le \pi \end{cases} \qquad (14)$$

By inverse Discrete Time Fourier Transform, the corresponding impulse response $g(\omega)$ of ideal low-pass filters can be represented as:

$$g(\omega) = \begin{cases} \dfrac{\sin(\omega_c k)}{\pi k}, & if\ \ k \ne 0 \\ \dfrac{\omega_c}{\pi}, & if\ k \ne 0 \end{cases} \qquad (15)$$

The specification of Kaiser low-pass filters is described by the sampling frequency f_s of the instrument and the four numbers $\{f_{pass}, f_{stop}, A_{pass}, A_{stop}\}$ shown in Figure 1, that is, the pass-band and stop-band frequencies and the desired pass-band and stop-band attenuations in dB (Orfanidis, 1996).

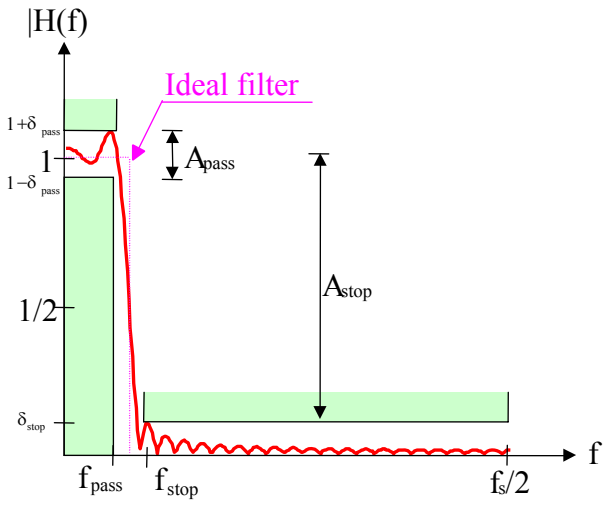

Figure 2 Kaiser window FIR low pass filter (Orfanidis, 1996)

The cut-off frequency f_s can be estimated as:

$$f_c = \frac{1}{2}\left(f_{pass} + f_{stop}\right) \tag{16}$$

The pass-band and stop-band deviation error are calculated as:

$$\delta_{pass} = \frac{10^{A_{pass}/20} - 1}{10^{A_{pass}/20} + 1}, \quad \delta_{stop} = 10^{-A_{pass}/20} \tag{17}$$

We choose the smaller one $\delta = \min(\delta_{pass}, \delta_{stop})$ and set $A = -20\log_{10}\delta$ in dB. Therefore, the final designed filter has equal pass-band and stop-band ripples. The Kaiser Window function can be expressed as (Orfanidis, 1996):

$$w(n) = \frac{I_0(\alpha\sqrt{n(2M-n)}/M)}{I_0(\alpha)}, \quad n = 0,1,\cdots,N-1 \tag{18}$$

where α is the window shape parameter, $I_0(\bullet)$ is a zero-order modified Bessel function of the first kind, and N the length of the filter. The window shape parameter and filter length can be calculated from A (see Orfanidis 1996 for more details). Finally, the windowed impulse response $h(n)$ and Kaiser FIR filter output $y(n)$ are obtained as:

$$h(n) = w(n)g(n-M), n = 0,1,\cdots,N-1 \tag{19}$$

$$y(n) = h(0)x(n),+h(1)x(n-1) + \cdots + h(N-1)x(n-N+1) \tag{20}$$

3. TEST DESCRIPTIONS

Figure 5 shows some pictures of the static test setup. The data were collected at the Inertial Lab at the University of Calgary, which is equipped with a thermal chamber. Static data sets were collected under different temperature points using two MEMS-based IMUs, namely MotionPakII and Crossbow AHRS300CC. The IMUs static data were sampled at 100 Hz at different temperature points and were saved on a card for post processing. The temperature ranges from -30 to 60 degree Celsius at 10 degree temperature interval. Thus, the performed test in this research covers the operational temperature of the IMUs.

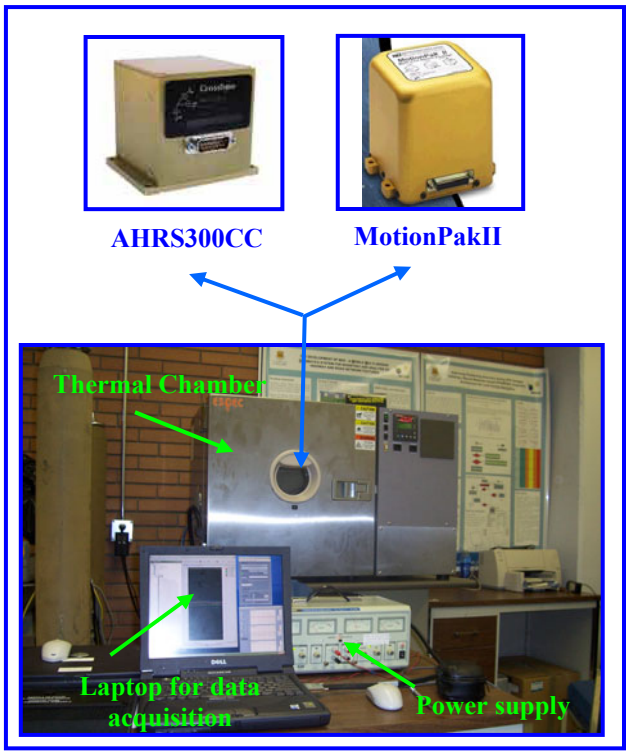

Figure 3 Test Description

4. RESULTS AND ANALYSIS

In this section, the performances of the MEMS inertial sensors are predicted from the results of the Allan variance estimates at different temperature points, whereas the LSSA is used to study the noise characteristics and to identify the sensors' stochastic model parameters. Also, the effect of de-noising the inertial data at different cut-off frequencies on the stochastic model is presented.

4.1. Allan Variance Analysis and Results

The raw outputs from different MEMS-based IMUs (i.e., voltage values) were first converted to acceleration and

angular rate. Then, the mean was removed before the analysis. Data include 1,080,000 samples (3 hours) and the data collected at a sampling interval of 0.01 s.

Allan variance results at different temperature points were analyzed to study the noise terms of MotionPakII and Crossbow AHRS300CC. Figure 4 and 5 illustrate a log-log plot of $\sigma(T)$ versus time at different temperature points. It is shown that the angular random walk is the dominant noise term and can be identified in the Allan plots.

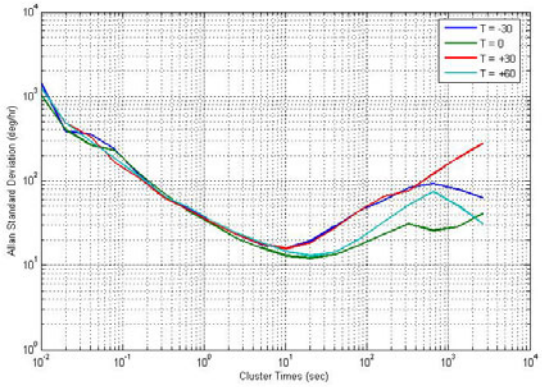

Figure 4 Allan variance for raw measurements of MotionPakII's Y gyro channel

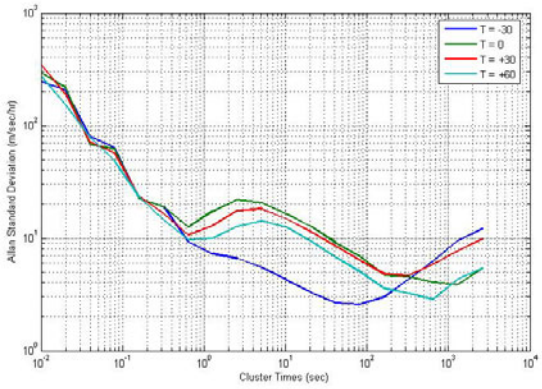

Figure 5 Allan variance for raw measurements of MotionPakII's Y accelerometer channel

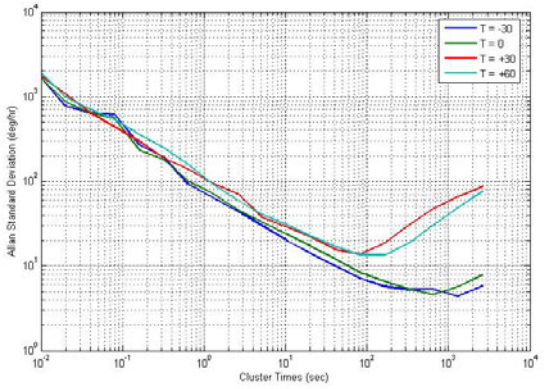

Figure 6 Allan variance for raw measurements of AHRS300CC's Y Gyro channel

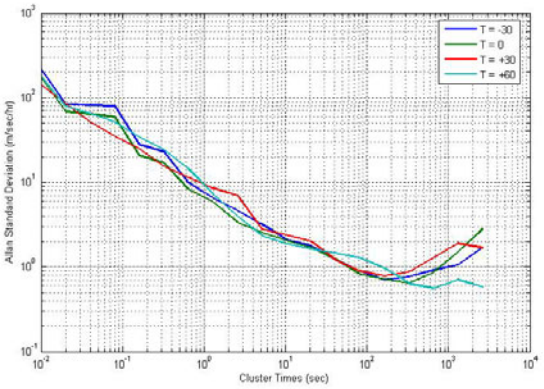

Figure 7 Allan variance for raw measurements of AHRS300CC's Y accelerometer channel

Using the above plots, the Allan variance values fit a straight line with slope of -1/2 (from parametric least square fitting). The fitted Allan variance line meets T=1 h at a value so-called Angular Random Walk (ARW) for gyros sensors and Velocity Random Walk (VRW) for accelerometers sensors. From the least squares fitting estimation results in Table 1, the variation of the estimated noise coefficients of gyros' and accelerometers' drifts in CrossBow AHRS400CC and MotionPakII are not small enough to be neglected in estimation process. As such a temperature-dependent stochastic model of the sensor drift is required. The disadvantage of Allan variance in this case is that the actual slope was not ideally at -1/2. In addition, no statistical tests can be performed to verify that the noise term is ARW and VRW for the gyro and accelerometer, respectively. The following sections discuss the analysis of the same dataset using the LSSA method to test statistically the Null hypothesis that the stochastic model is a random walk process and if not, what other alternative hypotheses can be identified using LSSA.

Table 1 Allan Variance Results (angular random walk (ARW) and velocity random walk (VRW)

Inertial/Temperature	Allan Variance Coefficient	
	Gyro (Y) ARW	Accelerometer (Y) VRW
MotionPakII	**Deg/√hr**	**m/s/√hr**
T=-30 ^{O}C	2.2292	0.4227
T = 0 ^{O}C	1.6224	0.4888
T= +30 ^{O}C	1.9547	0.5500
T= +60 ^{O}C	1.9549	0.4376
AHRS300CC	**Deg/√hr**	**m/s/√hr**
T=-30 ^{O}C	3.0994	0.3397
T=0 ^{O}C	2.6285	0.2696
T=30 ^{O}C	2.8262	0.2283
T=60 ^{O}C	3.0243	0.2811

4.2. LSSA Analysis Results Without De-noising

Two different methods were used to estimate the power spectral density for the static data series, namely Fast Fourier Transform (FFT) and LSSA. As mentioned above, the data points consisted of 1,080,000 samples (3 hours) at 0.01s sampling interval. The Fast Fourier Transform (FFT) was applied first followed by the Least Squares Spectral Analysis (LSSA). Figures 8 and 9 show the results of the FFT-based and LSSA-based power spectral densities (PSDs) in decibels (dB) for AHRS300CC's Y gyro channel at T=30 ^{0}C, respectively. From these figures, it is shown that the signal to noise ratio is small and almost constant with no statistically significant peaks.

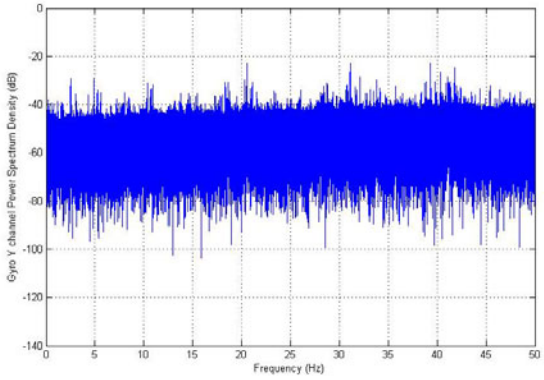

Figure 8 FFT-based PSD for raw measurements of AHRS300CC's Y Gyro channel (T=30^{O}C)

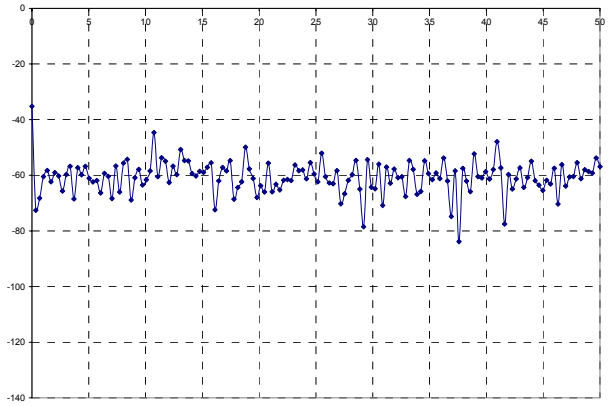

Figure 9 LSSA-based PSD for raw measurements of AHRS300CC's Y Gyro channel (T=30^{O}C)

Furthermore, the LSSA method was used to test the statistical significance of the Allan variance results and to identify the stochastic characteristics of the noise. The Null hypothesis H_o that the stochastic model is random walk or Auto Regressive models was made in LSSA for MotionPakII and Crossbow AHRS300CC Y Gyro and accelerometer channel. It was found that H_o is not accepted, thus the drift in both MEMS-based IMUs cannot be assumed to be a random walk process. However, it is statistically significant as a first order AR model. Table 2 shows the first order AR coefficient, C_{AR} which is statistically significant at the 99% confidence level (assuming that the first order AR form is of the form $b_{k+1} = C_{AR} b_k + e$). The estimated first order AR coefficients of the gyros' and accelerometers' drifts for CrossBow AHRS400CA and MotionPakII were temperature-dependent (see Figures 10 and 11).

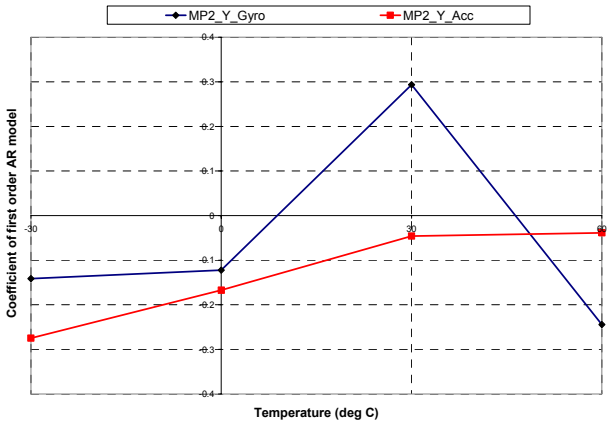

Figure 10 Coefficient of first order AR model at different Temperature points for MotionPakII Gyro/Accelerometer Y channel

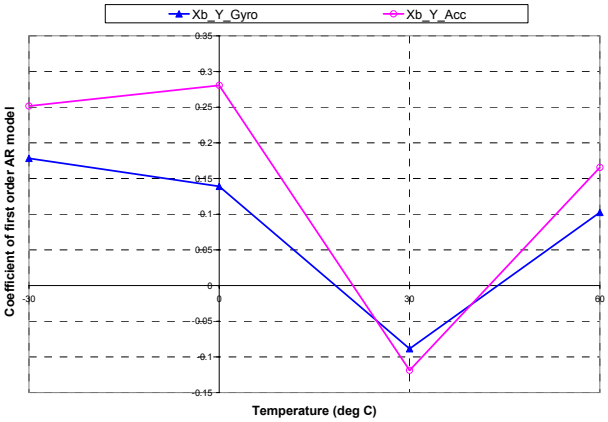

Figure 11 Coefficient of first order model at different Temperature points for AHRS300CC Gyro/Accelerometer Y channel

Table 2 Least Squares Spectral Results without pre-filtering (first order AR's coefficients, C_{AR})

Inertial/Temperature	First order AR's Coefficient	
	Gyro (Y)	Accelerometer (Y)
MotionPakII	**First order**	**First order**
T=-30 ^{O}C	-0.1413 ±0.0009	-0.2747 ±0.0009
T = 0 ^{O}C	-0.1223 ±0.0009	-0.1672 ±0.0009
T= +30 ^{O}C	0.2935 ±0.0009	-0.0460 ±0.0009
T= +60 ^{O}C	-0.2444 ±0.0009	-0.0388 ±0.0009
AHRS300CC	**First order**	**First order**
T=-30 ^{O}C	0.1783 ±0.0009	0.2515 ±0.0009
T=0 ^{O}C	0.13902 ±0.0009	0.2805 ±0.00092
T=30 ^{O}C	-0.0886 ±0.0009	-0.1188 ±0.0009
T=60 ^{O}C	0.1023 ±0.0009	0.1655 ±0.0009

4.3. LSSA Analysis and Results With De-noising Using Kaiser Window FIR Low Pass Filter

The effect of de-noising the MEMS-based inertial data, using a low pass filter, on the stochastic model was investigated. Three cut-off frequencies of 8 Hz, 16 Hz, and 24 Hz, respectively, were tested with the same attenuation values. Figure 12 shows the magnitude/phase response of Kaiser FIR filter with the following parameters: f_s = 100 Hz, f_{pass} = 14 Hz, f_{stop} = 18 Hz, A_{pass} = 0.0001 dB, and A_{stop} = 100 dB; this filter has small pass-band attenuation and somewhat long transition band. Figure 13 shows how the Kaiser FIR filter suppresses the high frequency magnitudes of PSD.

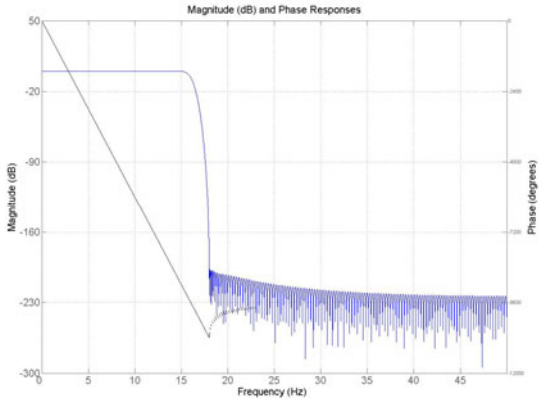

Figure 12 10 Kaiser Window FIR magnitudes (dB) and phase response

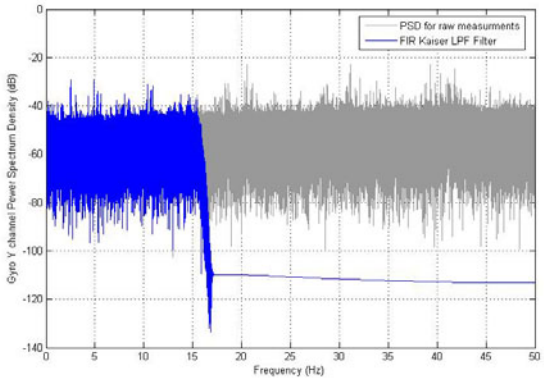

Figure 13 11 FFT-based PSD for measurements of AHRS300CC's Y Gyro channel versus de-noised values (T=30^{O}C and fc=16 hz)

The LSSA method was used again to identify the noise characteristics of the data after de-noising at three cut-off frequencies (8 Hz, 16 Hz, and 24 Hz). The H_o hypothesis of random walk or auto-regressive models was made for MotionPakII and Crossbow AHRS300CC Y Gyro and accelerometer channel. Tables 3 through 5 show the first order AR coefficients, C_{AR} , obtained from the LSSA method at 99% confidence level. Similar to the results presented above, it was found that the drift in both MEMS-based IMUs is not statistically significant as random walk process; however, it is statistically significant as a first order AR model. Also, it was found that the estimated first order AR coefficients of the gyros' and accelerometers' drifts for both IMUs are still temperature-dependent. In addition, the AR coefficient is dependent on the chosen cut-off frequency in the Kaiser FIR filter (Figures 14 and 15 illustrate) and should be considered in the estimation process.

Table 3 Least Squares Spectral Results with de-noising at fc=8 Hz (first order AR's coefficients, C_{AR})

Inertial/Temperature	First order AR's coefficient	
	Gyro (Y)	Accelerometer (Y)
MotionPakII	**First order**	**First order**
T=-30 ^{O}C	- 0.9649 ±0.0003	- 0.9559 ±0.0003
T = 0 ^{O}C	- 0.9684 0.0003	- 0.9776 ±0.0003
T= +30 ^{O}C	-0.9468 ±0.0003	-0.9549 ±0.0002
T= +60 ^{O}C	- 0.9758 ±0.0003	- 0.9623 ±0.0003
AHRS300CC	**First order**	**First order**
T=-30 ^{O}C	- 0.9567 ±0.0003	- 0.9499 ±0.0003
T=0 ^{O}C	- 0.9507 ±0.0003	- 0.9468 ±0.0003
T=30 ^{O}C	-0.9705 ±0.0002	-0.965680 ±0.0003
T=60 ^{O}C	- 0.9659 ±0.0002	- 0.9648 ±0.0003

Table 4 Least Squares Spectral Results with de-noising at fc=16 Hz (first order AR's coefficients, C_{AR})

Inertial/Temperature	First order AR's coefficient,	
	Gyro (Y)	Accelerometer (Y)
MotionPakII	**First order**	**First order**
T=-30 ^{O}C	- 0.9280 ±0.0004	- 0.8788 ±0.0004
T = 0 ^{O}C	- 0.9107 ±0.0004	- 0.8795 ±0.0004
T= +30 ^{O}C	- 0.9013 ±0.0004	- 0.8730 ±0.0004
T= +60 ^{O}C	- 0.8662 ±0.0004	- 0.7934 ±0.0004
AHRS300CC	**First order**	**First order**
T=-30 ^{O}C	- 0.8956 ±0.0004	- 0.9095 ±0.0004
T=0 ^{O}C	- 0.8752 ±0.0004	- 0.8980 ±0.0004
T=30 ^{O}C	- 0.8510 ± 0.0004	- 0.8450 ±0.0004
T=60 ^{O}C	- 0.8601 ±0.0004	- 0.8684 ±0.0004

Table 5 Least Squares Spectral Results with de-noising at fc=24 Hz (first order AR's coefficients, C_{AR})

Inertial/Temperature	First order AR's coefficient, C_{AR}	
	Gyro (Y)	Accelerometer (Y)
MotionPakII	**First order**	**First order**
T=-30 ^{O}C	- 0.7786 ±0.0006	- 0.3810 ±0.0006
T = 0 ^{O}C	- 0.7365 ±0.0006	- 0.3571 ±0.0006
T= +30 ^{O}C	-0.8054 ±0.0006	- 0.3736 ±0.0006
T= +60 ^{O}C	- 0.5690 ±0.0006	- 0.4425 ±0.0006
AHRS300CC	**First order**	**First order**
T=-30 ^{O}C	- 0.7257 ±0.0006	- 0.7598 ±0.0006
T=0 ^{O}C	- 0.6581 ±0.0006	- 0.7621 ±0.0006
T=30 ^{O}C	- 0.6004 ±0.0006	- 0.5801 ±0.0006
T=60 ^{O}C	- 0.6927 ±0.0006	- 0.7481 ±0.0006

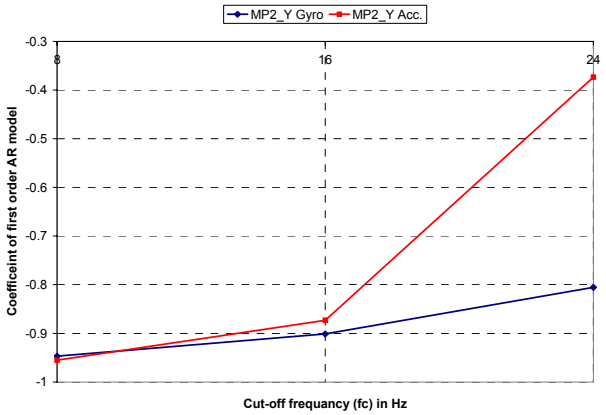

Figure 14 Coefficient of first order model for MotionPakII at different cut-off frequencies (fc) and at 30 ^{0}C Temperature

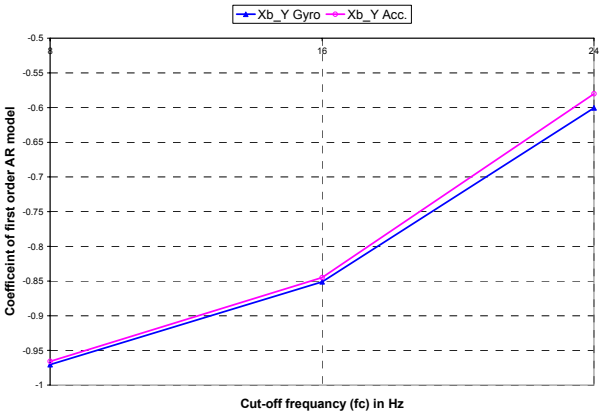

Figure 15 Coefficient of first order model for AHRS300CC at different cut-off frequencies (fc) and at 30 ^{0}C Temperature

CONCLUSIONS AND RECOMMNDATIONS

This paper investigated the effect of changing the temperature points on the MEMS inertial sensors noise models using Allan variance and LSSA. Allan variance can be used to identify the noise characteristics of MEMS-based inertial sensors. The method, however, does not verify the results, through, for example, statistical testing. LSSA, on the other hand, can be used to study the noise characteristics and to identify the sensors' stochastic model parameters. The LSSA estimation results of static data sets collected under different temperature points using two MEMS-based IMUs, MotionPakII and Crossbow AHRS300CC, showed that:

1. The drift in both MEMS-based IMU cannot be modeled as random walk (not statistically significant). On the contrary, an autoregressive (AR) model of first order is statistically significant

2. The estimated first order AR coefficients of gyros' and accelerometers' drifts are temperature-dependent.

The effect of de-noising the inertial data on the parameters of the stochastic model was also investigated, when the Kaiser FIR low pass filter was used. The LSSA estimation results of the same data sets, at different cut-off frequencies, showed that the above two conclusions are still valid. In addition, the estimated first order AR coefficient for both gyro and accelerometer drifts is dependent on the chosen cut-off frequency.

ACKNOWLEDGMENTS

This research was supported partially by the Natural Sciences and Engineering Research Council (NSERC) of Canada and by the GEOIDE National Centre of Excellence (Canada). The data used in this paper were collected at the Inertial Lab of the University of Calgary lead by Prof. Naser El-Sheimy.

REFERENCES

Abdel-Hamid, W. (2005), "Accuracy Enhancement of Integrate MEMS-IMU/GPS Systems for Land Vehicular Navigation Applications." PhD Thesis, Department of Geomatics Engineering, University of Calgary, Calgary, Alberta, Canada, UCGE Report No. 20207.

Abdel-Hamid, W., N. El-Sheimy, and G. Lachapelle (2003), "Thermal and Noise Characteristics of MEMS Inertial Sensors." Proceedings of NTM-GPS, 22-24 January, Anaheim, CA, USA, CD-ROM, pp. 641-648.

Gelb, A. (1974), "Applied Optimal Estimation." The M.I.T. Press, Cambridge, Massachusetts.

Hou, H. and N. El-Sheimy (2003), "Inertial Sensors Errors Modeling Using Allan Variance.", The US Institute of Navigation, ION GPS/GNSS 2003 Proceedings, pp. 2860-2867, Sep 9-12, Portland, 2003.

IEEE Std. 647-1995 (1998), "IEEE Standard Specification Format Guide and Test Procedure for Single-axis Interferometric Optic Gyros."

Mikhail, EM. (1976), "Observations and Least Squares." Thomas Y. Crowell Company, New York, 1976.

Nassar, S. (2003), "Improving the Inertial Navigation System (INS) Error Model for INS and INS/DGPS Applications." PhD Thesis, Department of Geomatics Engineering, University of Calgary, Calgary, Alberta, Canada, UCGE Report No. 20183.

Orfanidis, S. J. (1996), "Introduction to Signal Processing," Prentice-Hall

Pagiatakis, SD. (1999), "Stochastic significance of peaks in the least-squares spectrum." Journal of Geodesy 73: 67-78.

Park, M. (2004), "Error Analysis and Stochastic Modeling of MEMS based Inertial Sensors for Land Vehicle Navigation Applications.", M. SC. Thesis, The University of Calgary, Department of Geomatics Engineering, Calgary. UCGE Report No. 20194.

Skaloud, J. (1999), "Optimizing Georeferencing of Airborne Survey Systems by INS/DGPS." Ph.D. Thesis, Dept. of Geomatics Eng., The University of Calgary, Calgary, Alberta, Canada.

Shin, E. (2001), "Accuracy Improvement of Low Cost INS/GPS for Land Application." M.Sc. Thesis, The University of Calgary, Department of Geomatics Engineering, Calgary, Alberta, UCGE Report No. 20156.

Vanícek, P (1969), "Approximate Spectral Analysis by Least-squares Fit." Astrophysics and Space Science 4:387-391.

Vanícek, P., EJ. Krakiwsky (1986), "Geodesy: The Concepts. North Holland." Amsterdam (Second Edition).